

# A practical approach for the separation of interfacial toughness and structural plasticity in a delamination growth experiment

M. Kolluri · J. P. M. Hoefnagels ·  
J. A. W. van Dommelen · M. G. D. Geers

Received: 9 October 2011 / Accepted: 11 July 2013 / Published online: 30 July 2013  
© Springer Science+Business Media Dordrecht 2013

**Abstract** Interfacial delamination is a key reliability challenge in composites and micro-electronic systems due to (high density) integration of dissimilar materials. Predictive finite element models require the input of interface properties, often determined with an interface delamination growth experiment with (nearly) constant process zone, relying on the assumption of no permanent deformation in the sample structure layers. However, much evidence in the literature exists that plasticity often does occur in the sample structure during delamination experiments, which should be adequately dealt with to obtain the real interface fracture toughness that is independent of the thickness of the two sample arms. This paper presents a practical approach for the separation of interfacial toughness and structural plasticity in a delamination growth experiment on a double-cantilever beam specimen involving only small-scale plasticity at the interface. The procedure does not require knowledge of the constitutive behavior of the adherent layers. It only deals with the separation of structural plasticity in the adherents, whereas small-scale plasticity in connection with ductile interface

fracture is lumped into the interface fracture toughness. The proposed approach was numerically verified for one set of parameters. Experimental assessment of the approach on industrially-relevant copper lead frame–molding compound epoxy interface structures showed a correction of the interface fracture toughness of more than a factor of two, demonstrating the potentially significant errors induced by plastic deformation of the sample structure during delamination experiments.

**Keywords** Plasticity · Cohesive zone · Critical energy release rate · Delamination · Interface toughness · Work of separation

## List of symbols

$a$	Crack length
$\Delta a$	Crack length increase
$w$	Width of the sample
$K$	Global unloading stiffness
$u$	Displacement
$u_p$	Total retained opening
$u_{p,int}$	Retained opening due to interface plasticity
$u_{p,struct}$	Retained opening due to plasticity in the sample structure
$\Phi_{tot}$	Total work done in a loading–crack growth–unloading cycle

M. Kolluri  
Materials Innovation Institute (M2i), Mekelweg 2,  
P.O. Box 5008, 2600 GA Delft, The Netherlands

M. Kolluri · J. P. M. Hoefnagels (✉) ·  
J. A. W. van Dommelen · M. G. D. Geers  
Department of Mechanical Engineering,  
Eindhoven University of Technology,  
Den Dolech 2, 5612AZ Eindhoven, The Netherlands  
e-mail: j.p.m.hoefnagels@tue.nl

$\Gamma_o$	Energy consumed by breaking the chemical bonds at the interface
$\Gamma_{p,int}$	Plastic dissipation in the remote wake associated with interface fracture
$\Phi_{ese,int}$	Elastically stored energy associated with interface plasticity
$\Phi_{int}$	Interface fracture energy ( $= \Gamma_o + \Gamma_{p,int}$ )
$\Phi_{p,struct}$	Plastic dissipation in the sample structure due to bending
$\Phi_{ese,struct}$	Elastically stored energy associated with structural plasticity
$P$	Load
$x$	Section length of the sample
$u_n$	Crack opening displacement (COD)
$\delta$	Critical displacement (CZ parameter)
$\phi$	Interface fracture toughness (CZ parameter)
$\delta_{pl}$	Plastic limit (CZ parameter)
$T_{max}$	Maximum traction (CZ parameter)
$\Delta_{eff}$	Effective maximum separation of a CZ
$K_i^o$	Initial interface stiffness of a CZ
$K_i$	Interface stiffness of a CZ
$d$	Damage parameter

## 1 Introduction

Interfacial delamination is a key reliability issue in (laminate) composites (e.g. Todoroki et al. 2005; Davies et al. 2006; Kim and Mai 1991) and micro-electronic systems (e.g. van der Sluis et al. 2007; van Driel et al. 2005), where (high density) integration of dissimilar materials is required to achieve superior mechanical, physical and functional properties. As a consequence, identification of interfaces which are prone to delamination is important for the design and optimization of these systems. Hence, predictive models that can accurately capture the failure mechanisms of the interfaces are required for adequate design of these products. These models rely on a detailed characterization of the interface properties with an understanding of failure mechanics from dedicated experiments. Among all relevant interface properties, the interface fracture toughness, representing the amount of energy per unit area that is absorbed by the interface upon fracture, is perhaps the key parameter for mod-

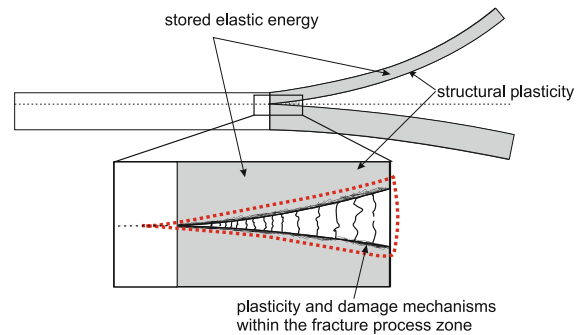


**Fig. 1** Schematic diagram of the fully unloaded interface sample illustrating the damage and plasticity mechanisms within the fracture process zone (*dashed envelope*) at the interface and permanent deformation in the structural layers of the sample (structural plasticity). Both interface and structural plasticity result in a stored elastic energy in the sample structure in an unloaded state

eling these interfaces. For a brittle interface between two perfectly brittle adherents, this fracture energy is approximately equal to the surface energy (needed for the creation of new surfaces). On the other hand, for interfaces between deformable materials, the formation of the new surfaces often also triggers dissipative mechanisms, such as damage and plasticity, in the adjoining materials in the immediate vicinity of the interface, identified as the fracture process zone as shown in Fig. 1. Hereafter, the plasticity within the process zone at the interface is referred to as interface plasticity. In this case, the surface energy and the energy spent for the fracture processes within the fracture process zone together contribute to the interface fracture toughness. However, the measured value of the interface fracture toughness, which is the characteristic property of the interface under small-scale yielding conditions at the crack tip, should be independent of the geometry of the adjoining material layers.

Traditionally, linear elastic fracture mechanics (LEFM) based techniques (Soboyejo et al. 1999; Davidson and Sundararaman 1996; Rikards et al. 1998; Blanco et al. 2006; Valoroso and Fedele 2010) are widely employed to experimentally characterize interface fracture toughness. LEFM based techniques are suitable for characterization of brittle interfaces under the small-scale yielding conditions. However, for characterization of a ductile interface behavior (large fracture process zone), LEFM based approaches can not be employed even under small-scale yielding conditions because of non-singular stress fields at the crack tip. Delamination growth experiments (Biel and Stigh 2010; Thijsse et al. 2008) resolve some of these issues

and are able to characterize the interface fracture toughness of interface structures for both small and large fracture process zones. In delamination growth experiments, the full load versus displacement response is recorded during initiation and propagation of delamination starting from an initial precrack. A schematic load–displacement diagram illustrating the initiation and propagation regimes is shown in Fig. 2a. The necessary condition for the delamination growth experiments is that the geometry of the process zone should remain constant during the crack propagation regime. That means, once the process zone is fully developed (i.e. after the crack initiation regime), the local crack opening geometry within the process zone should remain constant with increasing crack length and, therefore, the developed process zone moves along the interface upon further loading (i.e. in the propagation regime) without any changes in deformation field and elastically stored energy around the process zone. Then, the interface fracture toughness is simply calculated from the energy needed to propagate a fully developed crack per unit of delaminated area, i.e. the energy spent in one loading–unloading cycle (hashed region in Fig. 2a), divided by the sample width,  $w$ , times the crack length increase (i.e.  $\Delta a = a_2 - a_1$ ).<sup>1</sup> If the delamination setup allows for in-situ (microscopic) visualization of the crack propagation and thus accurate determination of the crack length increase for a constant crack opening geometry (e.g. Kolluri et al. 2009; Kolluri et al. 2011), then only the measurement uncertainties in force, displacement, and crack length affect the measured interface fracture toughness without contributions of any model assumptions. Without in-situ visualization,  $a_2 - a_1$  can still be obtained either by ex-situ crack length examination before and after the loading–unloading cycle, or from the reduction in global unloading stiffness  $K$  of the partly delaminated specimen (Thijsse et al. 2008). In all cases, the uncertainties involved with manufacturing of the precrack and the initial development of the process zone are avoided by ignoring the crack initiation regime of the load–displacement response.

Similar to LEFM approaches, delamination growth experiments intrinsically assume that the supplied energy to trigger delamination growth is stored elastically in the structure (e.g. the delaminating layers

composing the specimen structure), without any permanent deformation of the sample layers. In such a situation, without any plasticity mechanisms within the fracture process zone of the interface, the unloading curve starting at a crack length  $a$  should return to the origin (along a straight line). This behavior is indeed often observed in experiments, e.g. curve 1 in Fig. 2b, showing the load–displacement response measured from a mode I delamination experiment on a coated copper lead frame (CuLF)–molding compound epoxy (MCE) interface (Kolluri et al. 2011).

In the absence of permanent structural deformation, any retained opening after complete unloading should be the result of plasticity of the material within the fracture process zone during the separation of the two materials. In reality, however, during the delamination experiment there can be plastic bending of the sample structure (referred as structural plasticity, see Fig. 1) leading to an additional mechanical work due to structural plastic dissipation and associated stored elastic energy besides the energy spent for the actual delamination process and resulting in additional retained opening after complete unloading. That means that the observed retained opening in curve 2 of Fig. 2b (measured for a similar sample as for curve 1 but without interface coating) might originate from either plasticity mechanisms within the fracture process zone at the interface or from structural plasticity of the sample layers or from both. Figure 2c shows a schematic load–displacement response of an interface system that exhibits plasticity mechanisms within the fracture process zone at the interface, as well as structural plasticity. This figure illustrates the possible resulting contributions of retained opening due to the plasticity within the fracture process zone at the interface ( $u_{p,int}$ ) and due to the permanent deformation of the sample structure ( $u_{p,struct}$ ) to the measured (total) retained opening.

Similar to the Hutchinson's (Wei and Hutchinson 1997) I-integral approach of quasi-static stable crack growth in elastic-plastic solid, the presented method also relies on an energy-balance relation for a quasi-static stable crack growth problem. The total energy balance equation (per unit increase in crack area) for a steady state quasi-static delamination problem can be written as follows,

$$\Phi_{tot} = \Gamma_{\circ} + \Gamma_{p,int} + \Phi_{ese,int} + \Phi_{p,struct} + \Phi_{ese,struct}, \quad (1)$$

<sup>1</sup> It should be noted that the delamination growth experiments are devised for measurement of the propagation fracture toughness.

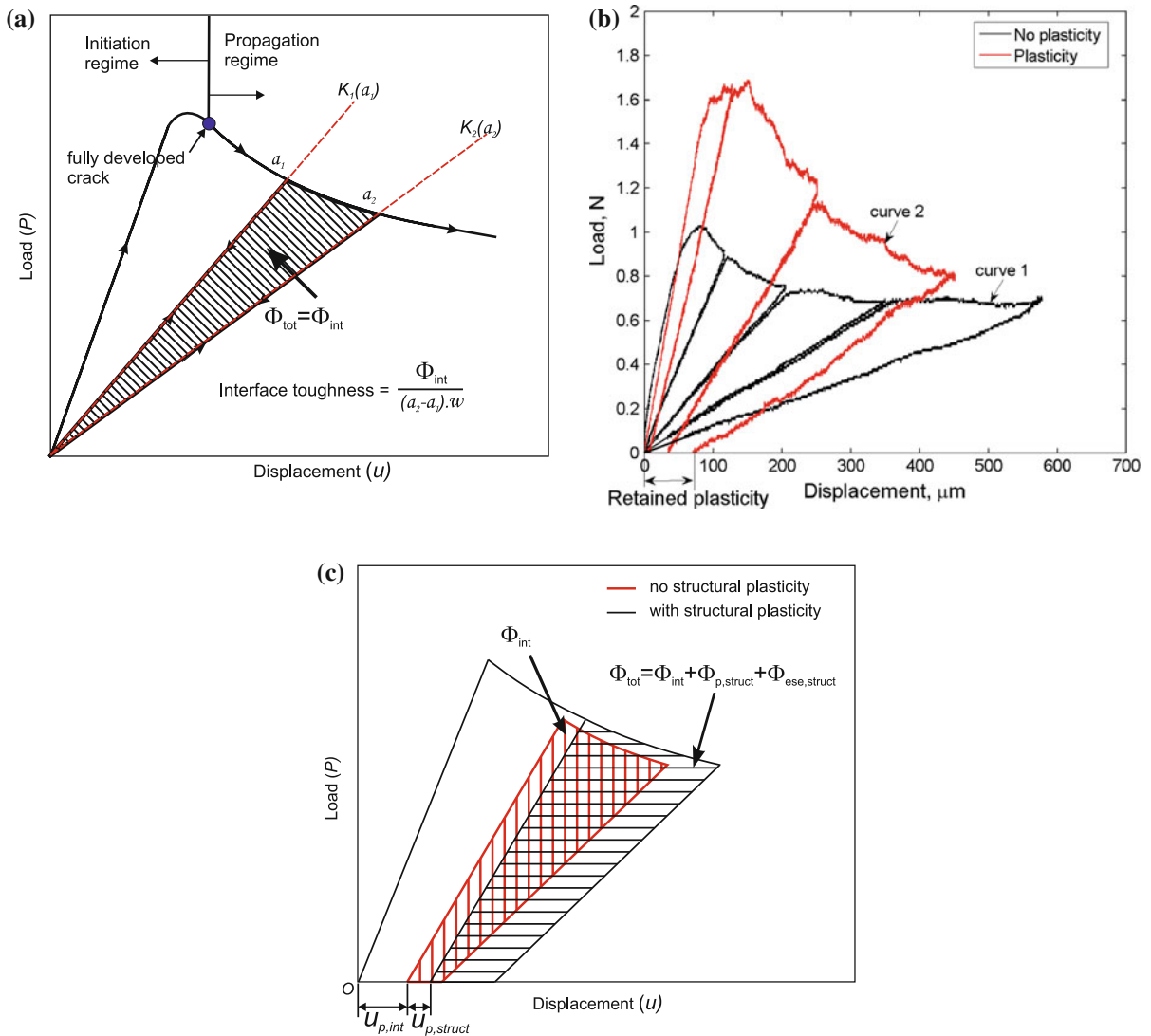


**Fig. 2** Illustration of delamination growth experiments. (a) Schematic plot illustrating how the interface fracture toughness is obtained either from the energy spent in one loading–delamination–unloading cycle (hashed area) with known increase in crack length or with estimated stiffness lines for chosen crack lengths. (b) Experimental load–displacement curves exhibiting no plasticity (curve 1) after unloading and significant (retained) plasticity (curve 2) after unloading (Kolluri et al. 2011). (c) A schematic load–displacement response curve of an

interface system that has plasticity mechanisms within the fracture process zone at the interface, and shows structural plasticity as well. Consequently, the resultant retained opening is due to plasticity within the fracture process zone at the interface ( $u_{p,int}$ ) and due to the permanent deformation of the sample structure ( $u_{p,struct}$ ). The hashed regions indicate the total dissipated energy during one loading–delamination–unloading cycle in cases of with and without structural plasticity

where,  $\Gamma_o$  is the work per unit area consumed by breaking the chemical bonds at the interface (i.e. energy spent to create new surfaces),  $\Gamma_{p,int}$  represents plastic dissipation in the remote wake associated with interface fracture and  $\Phi_{ese,int}$  is the corresponding elastic stored energy,  $\Phi_{p,struct}$  is plastic dissipation in the sample structure (e.g. due to bending) and  $\Phi_{ese,struct}$

is elastic stored energy due to the plasticity in the sample structure. Of the measured total work of separation ( $\Phi_{tot}$ ), only the sum of  $\Gamma_o + \Gamma_{p,int}$  (which equals the interface fracture energy,  $\Phi_{int}$ ) should be included in the measured thickness-independent interface fracture toughness for a small-scale plasticity problem, but not the energy that is plastically dissipated in the

sample structure ( $\Phi_{p,struct}$ ) and the associated elastically stored energy ( $\Phi_{ese,struct}$ ). The change in  $\Phi_{ese,int}$  is (approximately) zero for a steady state quasi-static crack growth problem with a negligible change in process zone geometry. However, it is not known a priori whether both structural plastic dissipation and plastic dissipation within the fracture process zone are present. Therefore, the contribution of structural plastic dissipation and resulting stored elastic energy should be identified quantitatively and separated in order to obtain a correct value of the interface fracture toughness. The approach presented in this paper aims to separate ( $\Gamma_o + \Gamma_{p,int}$ ) from ( $\Phi_{p,struct} + \Phi_{ese,struct}$ ) for delamination problems involving small-scale plasticity in connection with ductile interface fracture and structural plasticity in the adherents induced by beam bending. Contrastingly, the I-integral approach for large-scale plasticity problems assumes  $\Phi_{p,struct} + \Phi_{ese,struct} = 0$  and aims to separate  $\Gamma_o$  from  $\Gamma_{p,int} + \Phi_{ese,int}$ , because for large-scale plasticity problem there exists no thickness-independent interface fracture toughness, i.e.  $\Gamma_{p,int}$  and  $\Phi_{ese,int}$  increase continuously during ongoing delamination.

In the literature, considerable emphasis was given to understand and separate the influence of structural plasticity on interface fracture toughness measurements. Many studies (Tvergaard and Hutchinson 1993, 1996; Wei and Hutchinson 1997, 1998; Yang and Thouless 2001) were performed to understand the influence of structural plasticity on the mode dependent fracture toughness of an interface between dissimilar elastoplastic solids. All these studies predicted that plastic deformation outside of the fracture process zone leads to an increase in apparent fracture toughness. Later, Thouless and co-workers (Yang et al. 1999) performed a numerical analysis of interface fracture in adhesively bonded beams failing with extensive plastic deformation, using an embedded process zone model (EPZ) developed by Tvergaard and Hutchinson (1992), and they found the EPZ parameters to be unaltered by plasticity in the layers of the sample structure. This opens up the possibility to obtain the fracture toughness from the experiment in the presence of structural plasticity. Indeed, for the case of pure bending moment-driven delamination experiments, Thouless et al. (1998) were able to derive an analytical solution for the fracture toughness of an adhesively bonded double-cantilever beam (DCB) that fails with extensive plastic deformation of the adherents, assuming a

plastic power law hardening to describe the structural plasticity. Further analysis on pure bending moment-driven delamination experiments in conjunction with plastically deforming layers was performed by Stigh and co-workers (Andersson and Stigh 2004; Salomonsson and Stigh 2008). All these efforts indeed indicate that the plastic dissipation in the sample structure should be separated from the total steady state work of separation (during a delamination experiment), to obtain the interface fracture toughness that is independent of the geometry of the adjoining material layers.

The studies cited above are valuable to understand and evaluate the influence of structural plasticity on interface fracture toughness measurements, but they require either analytical solutions or numerical simulations with a representative plastic description of the adherent material layers. This does not enable a direct interpretation of data from delamination experiments to obtain the correct value of the interface fracture toughness. In contrast, the methodology presented in this paper is based on total energy balance of the complete sample in a mode I delamination growth experiment, where the retained structural opening resulting from the structural plasticity is directly measured and employed to separate the interface fracture energy from the total work done in a loading–crack growth–unloading cycle. Therefore, this methodology requires neither an analytical solution or a numerical simulation nor the constitutive behavior of the adherents. However, the proposed methodology is applicable only for delamination growth experiments, in which loads are applied to trigger delamination and for which the geometry of the process zone remains constant during crack propagation. In addition, the approach can only be used to compensate for energy dissipation due to structural plasticity leading to a permanent curvature. Finally, it is also noted that the proposed approach is not applicable when the structural arms of the sample undergo plastic deformation during unloading (i.e. reverse plasticity) and when there are any dissipative mechanisms causing non-negligible hysteresis in the global un- and reloading response.

The article is organized as follows. First, a practical approach is hypothesized to separate the contribution of structural plastic dissipation and associated stored elastic energy from the total measured work of separation during a delamination growth experiment on a

DCB specimen. Then, the proposed approach is verified for one set of parameters employing finite element numerical simulations with cohesive zone elements (at the interface), using arbitrary constitutive properties of the bulk material as well as the interface. Finally, to assess the proposed approach experimentally, two experiments were conducted to measure the interface fracture toughness of two identical industrially relevant CuLF–MCE structures with one sample showing significant structural plastic dissipation (with a thin CuLF layer) and the another showing negligible plastic deformation (due to a thick CuLF layer).

## 2 Procedure to extract interface fracture toughness

In this section, the methodology for the separation of structural plastic dissipation and associated elastic stored energy from the total measured work of separation during a delamination growth experiment is presented, as well as the underlying assumptions. The key principle relies on the reconstruction of the fictitious force–displacement response (in the crack propagation regime) that would have been measured in the absence of structural plasticity, for which the interface fracture toughness can be determined directly as explained earlier in Fig. 2b. To be able to reconstruct this fictitious structural plasticity-free force–displacement curve, the following assumptions, which will be numerically verified in the next section, are made:

- (1) Plasticity in the sample structure has no influence on the global (unloading) stiffness, for a given crack length, with or without plasticity within the fracture process zone at the interface.
- (2) For a given crack length, the critical global load required for a crack to grow with or without structural plasticity is the same (i.e. the load depends on the interface fracture resistance only).

In addition, the key requirements for this approach to be valid are,

- (i) the geometry of the process zone remains unchanged during crack propagation, which anyway is a necessary condition for delamination growth experiments in general as mentioned earlier,
- (ii) the structural arms of the sample should not undergo plastic deformation during unloading

(i.e. reverse plasticity), because reverse plasticity changes the global unloading stiffness making assumption 1 no longer valid, and

- (iii) the approach can only be used to compensate for energy dissipation due to structural plasticity leading to a permanent curvature because the reconstruction of the plasticity-free force–displacement curve will be done using the retained curvature profile of the sample structure.

### 2.1 Case 1: Structural plasticity, no plasticity in the fracture process zone at the interface

As already discussed in the previous section, the observed retained opening can originate from either plasticity mechanisms within the fracture process zone at the interface or from structural plasticity of the sample layers or from both. In the case of only structural plasticity, the procedure for reconstruction of the force–displacement curve that corresponds to the (fictitious) case without structural plasticity is relatively simple using the above two assumptions. This is because the above two assumptions allow translation of each point on the force–displacement curve measured with structural plasticity to its plasticity-free equivalent such that unloading from that point to zero load leads to zero retained opening.

In Fig. 3, the black solid curve represents an experimentally measured load–displacement response during a loading–unloading experiment. Area  $ACDB$  represents the total work done ( $\Phi_{tot}$ ) during the crack growth of  $\Delta a = a_C - a_A$  between two consecutive unloadings. This total energy contains the interface fracture energy ( $\Phi_{int}$ ), the structural plastic dissipation ( $\Phi_{p,struct}$ ) and associated elastic stored energy ( $\Phi_{ese,struct}$ ). Using assumption 1, the global unloading stiffness lines  $AB$  and  $CD$  can be translated horizontally towards the origin over the distance  $OB$  and  $OD$  (i.e.  $u_{p,struct,B}$  and  $u_{p,struct,D}$ ), respectively, in order to find the points  $A'(u_{A'}, P_A)$  and  $C'(u_{C'}, P_C)$  where  $u$  and  $P$  indicate the displacement and load, respectively. The points  $X'(u_{X'}, P_X)$  between  $A'$  and  $C'$  (the dashed curve in Fig. 3) can be reconstructed using the relation,  $u_{p,struct,X} = u_{p,struct,A} + \frac{u_{p,struct,C} - u_{p,struct,A}}{u_C - u_A} (u_X - u_A)$ , which represents a scaled linear interpolation of  $u_{p,struct,X}$  between  $u_{p,struct,A}$  and  $u_{p,struct,C}$ . Now, the curve  $OA'C'$  represents the plasticity-free equivalent of the original curve, from which the inter-

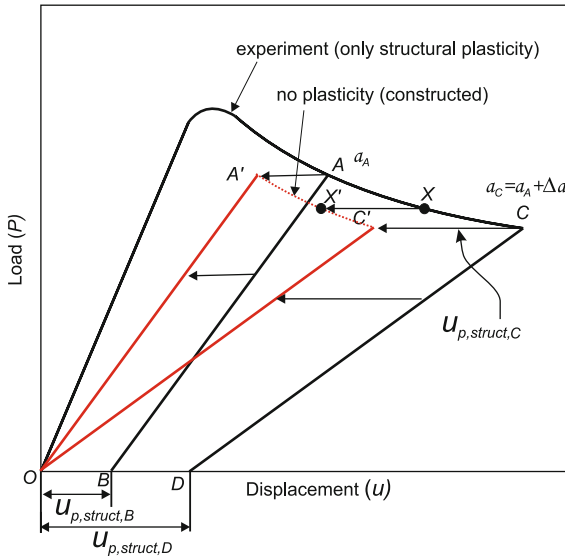


**Fig. 3** Schematic diagram illustrating the reconstruction of the virtual plasticity-free load–displacement response for a measurement in which only structural plasticity is present

face fracture energy  $\Phi_{int}$  can be determined directly as it is equal to the area  $OA'C'$ . As explained earlier,  $\Phi_{int}$  divided by the increase in crack length  $\Delta a$  and the width of the sample,  $w$ , yields the interface fracture toughness.

It is worth mentioning here that only  $\Delta a$  is needed (and not the absolute values of the crack lengths at the unloading points) to calculate the interface fracture toughness. This is important because the exact crack length also depends on the definition of a crack tip, whereas, the  $\Delta a$  can be obtained relatively easily with high accuracy for a steady state moving process zone, e.g. by matching displacement fields obtained with digital image correlation (DIC).

### 2.2 Case 2: Structural plasticity and plasticity within the fracture process zone at the interface

For the case of both structural plasticity and plasticity within the fracture process zone at the interface, the total energy dissipated between two consecutive unloadings for the crack to grow by  $\Delta a$  (area  $ACDB$  in Fig. 4) contains again the interface fracture energy ( $\Phi_{int}$ ), the structural plastic work ( $\Phi_{p,struct}$ ) and the elastic stored energy ( $\Phi_{ese,struct}$ ) in the sample resulting from structural plasticity. However, the total retained opening after complete unloading,  $u_p$ , is now

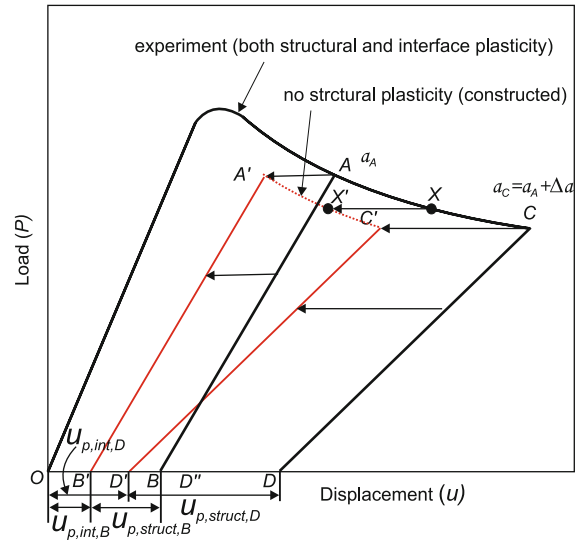


**Fig. 4** Schematic diagram illustrating the reconstruction of the virtual plasticity-free load–displacement response for a measurement in which both structural and interface plasticity are present

the sum of the retained opening due to structural plasticity  $u_{p,struct}$ , and the plasticity within the process zone  $u_{p,int}$ . An apparently stiffer global unloading response is seen when there is plasticity at the interface, because, for the *same* given global opening displacement, the effective crack length will be less in this case compared to the case of no-interface plasticity (Fig. 3). Therefore, the measured stiffness lines can no longer be translated to the origin ( $O$ ) as was done in the previous case.

To solve this problem, a practical approach, which relies only on experimental measurements, is proposed to separate the structural plastic dissipation  $\Phi_{p,struct}$  and the associated stored elastic energy ( $\Phi_{ese,struct}$ ) from the total work  $\Phi_{tot}$  to obtain the interface fracture energy  $\Phi_{int}$ . In this approach, first the individual contributions due to structural plasticity ( $u_{p,struct}$ ) and plasticity within the process zone at the interface ( $u_{p,int}$ ) to the total retained opening ( $u_p$ ) are identified for (at least) two unloading steps (explained below). Then, the experimental global unloading stiffness lines are translated towards the origin by the corresponding retained opening due to structural plasticity,  $u_{p,struct}$  (yet to be determined). This allows to identify (in the propagation regime) the virtual force–displacement curve equivalent to the no structural plasticity case. For example in Fig. 4, lines  $AB$  and  $CD$  are translated by  $BB'$  and  $DD'$  (i.e.  $u_{p,struct,B}$  and  $u_{p,struct,D}$ ), respectively, to find  $A'$  and  $C'$ . The points

$X'(u_{X'}, P_x)$  between  $A'$  and  $C'$  (the dashed curve in Fig. 3) can be obtained using the relation,  $u_{p,struct}$ ,  $X = u_{p,struct,A} + \frac{u_{p,struct,C} - u_{p,struct,A}}{u_C - u_A}(u_X - u_A)$ , as explained earlier in Sect. 2.1. Then, area  $A'C'D'B'$  represents the interface fracture energy  $\Phi_{int}$  for the crack to grow from  $a_A$  to  $a_C$ , which divided by  $\Delta a$  and  $w$  gives the interface fracture toughness.

Key part of this approach is the separation of the individual contribution of structural plasticity ( $u_{p,struct}$ ) and plasticity within the process zone at the interface ( $u_{p,int}$ ) from the total retained opening ( $u_p$ ), for which the following additional assumption is used:

- (3) Plasticity in the sample structure develops predominantly in the region surrounding the process zone since the stresses in the layers are the highest there (during delamination growth). This means that the plastic curvature at a certain position does not or only slightly change after the process zone has passed by, resulting in a smooth curvature profile of the delaminated beams.

The procedure for obtaining the retained opening due to structural plasticity involves the following steps. First, for each layer the retained crack opening displacement (COD) profile,  $u_n$ , (defined with respect to the undeformed interface, i.e.  $Ox_{end}$  in Fig. 5) of the fully unloaded sample at the end of the delamination test is determined. The retained COD profiles of both adherent bulk layers can be obtained, for example, from a recorded micrograph of the fully unloaded sample, e.g. using a digital imaging correlation (DIC) technique as shown in Sect. 4. The process zone and the region close to the process zone until the beginning of fully delaminated interface (referred to as region 1 in Fig. 5), are influenced by both plasticity in the process zone and structural plasticity, whereas the measured retained curvature in the layers in region 2 is the result of structural plasticity only. Region 3 and 4 in Fig. 5 represent the crack initiation and pre-crack regions, respectively. Region 2 can be fitted with a low order polynomial equation because plasticity in the sample structure results in a smooth curvature profile of the delaminated beams [according to assumption (3)]. Then the fitted polynomial can be extrapolated into Region I to identify the point  $a_c^{fit}$  on the undeformed sample axis  $Ox_{end}$ , see Fig. 5. The tangent of the fitted curve at  $a_c^{fit}$  extended to  $x = x_{end}$  reveals retained opening,  $u_{p,int}$ , at the end of the sample where the load was applied, as a result of the plasticity in the process

zone, i.e.  $u_{p,int} = (x_{end} - a_c^{fit}) \left[ \frac{d(u_n^{fit}(x=a_c^{fit}))}{dx} \right]$ . Next, the contribution of structural plasticity,  $u_{p,struct}$ , to the total retained opening,  $u_p$ , is recovered by  $u_{p,struct} = u_p - u_{p,int}$ . In Fig. 5, this procedure is illustrated for the top bulk layer. The same procedure is repeated for the bottom layer if both sample layers undergo permanent deformation during delamination. The total retained openings due to structural plasticity,  $u_{p,struct}$ , and due to the plasticity within the process zone,  $u_{p,int}$ , are obtained by adding the corresponding individual contributions from both layers. It is worth mentioning again that the condition of constant process zone geometry during crack propagation is necessary for the validity of the approach.

### 3 Numerical verification

In this section, first, the three assumptions made in the previous section are verified numerically using finite element simulations employing an interface cohesive zone (CZ) model that allows for modeling the irreversible unloading response that result from the combined damage and/or plasticity mechanisms within the process zone at the interface (Kolluri 2011). That means that all the dissipative (damage and plasticity) mechanisms within the fracture process zone are lumped into the interface behavior described with the cohesive zone model. A brief review of this CZ model is given in Sect. 3.1. After verification of the assumptions, the proposed approach to separate the structural plasticity contribution from the total energy dissipated during a delamination experiment is verified, in order to recover the correct interface fracture toughness value.

#### 3.1 Summary of the irreversible interface model

The combined plasticity–damage CZ model proposed by Kolluri (2011) allows for irreversible openings due to damage and/or plasticity. The combined (plasticity–damage) behavior depends on the ratio of the plastic energy and the total energy of separation using one additional parameter called the plastic limit,  $\delta_{pl}$ . The other parameters are standard ones (i.e. the interface fracture toughness  $\phi$  and critical displacement  $\delta$  characterizing the loading behavior of the traction–separation law). The plastic limit,  $\delta_{pl}$ , is defined such



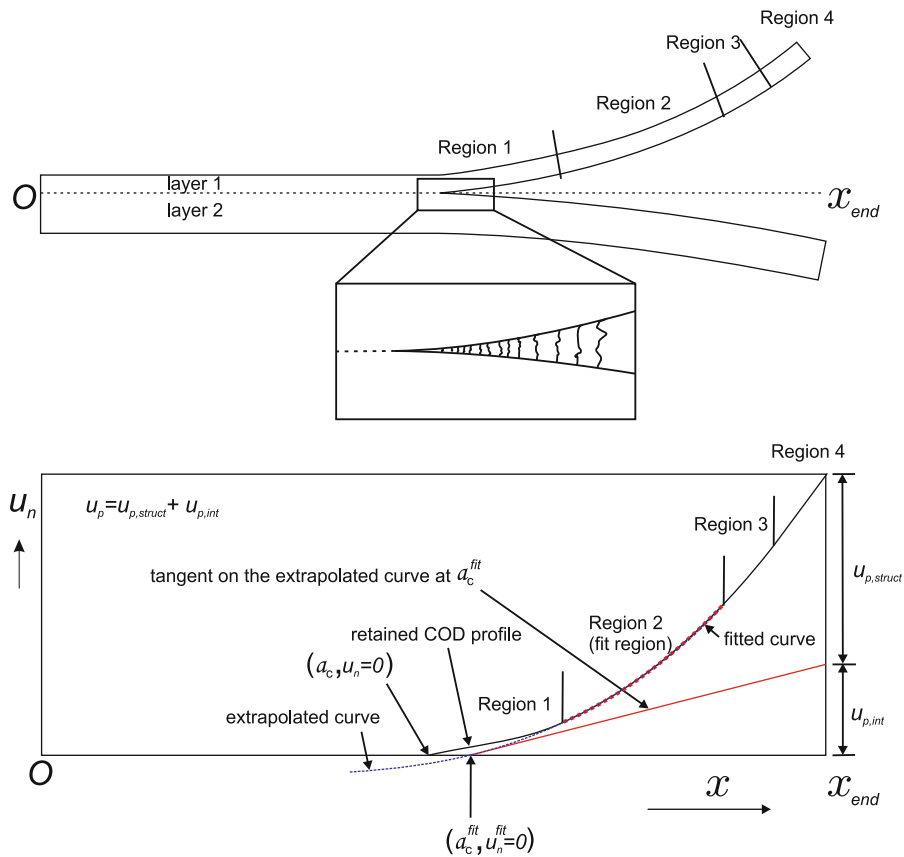


**Fig. 5** Schematic figure showing the fully unloaded sample (*top*) and the corresponding retained opening profile of the top layer (*bottom*) with respect to undeformed sample axis  $Ox_{end}$ . The figure also shows the four different regions of the delaminated sample, i.e. (1) the region influenced by both structural plasticity and plasticity within the fracture process zone, (2) the region where the measured retained curvature is influenced by struc-

tural plasticity only, (3) the crack initiation region, and (4) the pre-cracked region. Region 2 is fitted with a low order polynomial and extrapolated into region 1 to identify the point  $u_n^{fit}(a_c^{fit}) = 0$  intersecting  $Ox_{end}$ . Separation of structural plasticity,  $u_{p,struct}$ , and the plasticity within the process zone,  $u_{p,int}$ , is obtained by constructing a tangent to the extrapolated curve at  $a_c^{fit}$

that for an effective maximum separation  $\Delta_{eff}$  smaller than  $\delta_{pl}$ , the cohesive zone behaves fully elasto-plastic (i.e. the interface stiffness,  $K_i$ , remains equal to the initial stiffness,  $K_i^0$ ). Once the effective maximum separation exceeds  $\delta_{pl}$ , the plastically deformed cohesive zone damages elastically with further separation (i.e. the interface stiffness decreases with damage parameter  $d$ ), as presented in Fig. 6a. In this figure, this irreversible CZ behavior is used in conjunction with the improved Xu–Needleman CZ law for normal separation, which is used to describe the interface loading behavior.

Figure 6b shows that by varying the plastic limit from 0 to  $\infty$ , the irreversible interface behavior of the CZ can be varied from full damage to a mixture of

damage and plasticity to full plasticity. In this model, the compressive stiffness of the CZ is not influenced by the damage.

### 3.2 Verification of the assumptions and necessary conditions

In order to verify the assumptions made in the previous section as well as the necessary condition of a constant process zone geometry, finite element simulations of a mode I delamination test on a dissimilar bilayer interface sample are performed for four classes of material behavior for the interface and bulk, representing the behavior of the fracture process zone and

**Fig. 6** **a** The unloading behavior of the combined plasticity–damage CZ in normal opening above and below the plastic limit  $\delta_{pl}$ . **b** The influence of  $\delta_{pl}$  on the unloading behavior of the combined plasticity–damage CZ in normal opening

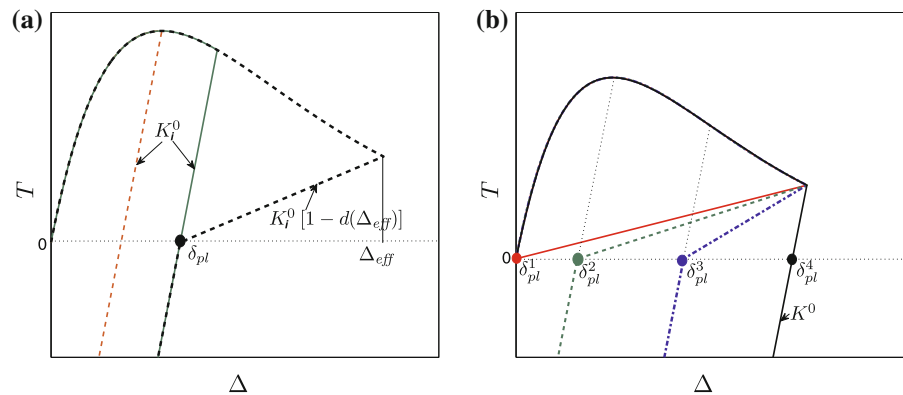
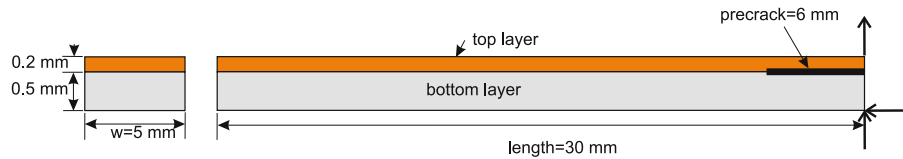


**Fig. 7** Geometry of the sample and the applied boundary conditions for simulations



sample structure, respectively, given in Table 1. A 2D finite element model of the bilayer sample with the geometry and boundary conditions given in Fig. 7 has been made. The mesh was selectively refined at the interface to avoid mesh size dependency on the final results. Four-node quadrilateral elements with a maximum size of 100  $\mu\text{m}$  and a minimum size of 1.6  $\mu\text{m}$  are used to model the top and bottom layers of the sample. The CZ elements are of the same size as the minimum element size of the bulk quadrilateral element, i.e. 1.6  $\mu\text{m}$ . Frictionless contact conditions were used between the two surfaces of the precrack region of the specimen. Simulations were performed by assuming plane strain conditions. The CZ model described in Sect. 3.1 was implemented, whereby a return mapping solution procedure<sup>2</sup> was employed to incorporate the plasticity. The behavior of the bottom layer is assumed to be elastic in all the simulations for simplicity. Hence, structural plasticity is only present in the top layer for simulations MB2 and MB4. The material properties of the two layers of the sample structure and the cohesive zone parameters of the interface used in the simulations are given in Table 2. The cohesive zone parameters of the interface are chosen such that there is considerable permanent deformation due to plasticity in the fracture process zone (for a clear influence of process zone

**Table 1** The four classes of interface (representing the fracture process zone) and bulk (representing the sample structure) material behavior used for the simulations

Class	Interface (fracture process zone)	Bulk (sample structure)
MB1	Full damage	Elastic
MB2	Full damage	Elasto-plastic
MB3	Partial damage—partial plasticity	Elastic
MB4	Partial damage—partial plasticity	Elasto-plastic

plasticity) and the interface strength is relatively low. Finally, the resulting load displacement responses from the simulations of the four different material classes are shown in Fig. 8.

To verify assumption 1, the (global) unloading stiffness,  $K$ , corresponding to a given crack length,  $a$ , should not be influenced by the presence of structural plasticity, with and without interface plasticity. Because of the complications in controlling two simulations with different material behavior to unload at exactly the same crack length, a direct comparison of global unloading stiffness values obtained from simulations with structural plasticity (MB2 and MB4) with those from simulations without structural plasticity (MB1 and MB3), respectively, is not possible. To circumvent this problem, the global unloading stiffness values of all four material behavior classes are plotted (in Fig. 9a) as  $K^{-1/3}$  versus the corresponding crack lengths  $a$  at each opening displacement (because  $K^{-1/3}$  should scale linearly with  $a$  when linear elas-

<sup>2</sup> Return mapping is a standard term in plasticity used for a method to solve the plasticity equations. In such methods, a fully elastic trial stress is mapped back to the yield surface in order to obtain the solution.

**Table 2** Material properties of the sample layers and cohesive zone parameters of the interface

Material parameters	Top layer	Bottom layer
Young’s modulus (GPa)	120	30
Poisson’s ratio	0.33	0.25
Yield stress (MPa)	67 (for MB2 and MB4)	–
Hardening parameter (GPa)	5 (for MB2 and MB4)	–
Cohesive zone parameters		
$\phi$ (J/m <sup>2</sup> )	4.7	
$\delta$ (μm)	3	
or $T_{max}$ (MPa)	0.576	
$\delta_{pl}$ (μm)	10 (MB1 and MB3)	

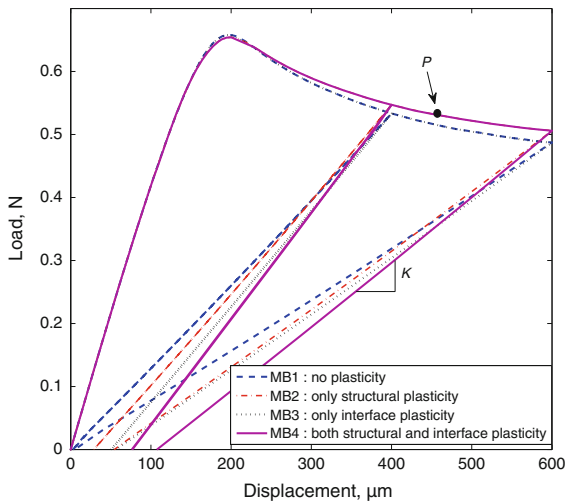


**Fig. 8** Load–displacement results from the finite element simulations of a mode I delamination test performed with the four classes of interface and bulk structural material behavior given in Table 1

tic beam theory would be valid). The data points from simulations with and without structural plasticity fall on one (quadratic) curve in the absence of interface plasticity (MB1 and MB2) (see Fig. 9a). Likewise, in the case with interface plasticity (MB3 and MB4), the simulations with and without structural plasticity fall on another (quadratic) curve. This demonstrates that there is indeed a negligible influence of structural plasticity on the global unloading stiffness in both cases, which verifies assumption 1. Note that the slight non-

linearity in relation between  $K^{-1/3}$  and  $a$  demonstrates that linear elastic beam theory oversimplifies the sample structure geometry.

To check assumption 2, the inverse of the critical load points on the delamination curve are plotted as a function of the corresponding crack lengths for both cases with and without structural plasticity as shown in Fig. 9b. The observed linear dependency between  $P^{-1}$  and  $a$  with the same slope for all cases (MB1 and MB3, MB2 and MB4) indicates that the critical load for delamination is the same for samples with and without structural plasticity.

To check the validity of assumption 3, the retained curvature after complete unloading of cycle 1 and cycle 2 for the case of MB4 is shown in Fig. 10a. The different regions of the retained opening profile (after cycle 2) are also identified on the curvature plot (Fig. 10b). This curvature graph shows that the retained structural plastic curvature in region 2 of delaminated specimen arms is approximately the same for both cycles, indicating that the plastic curvature stays nearly constant in time with further loading once the process zone has passed. Therefore, Fig. 10b shows that the structural layers of the sample deform plastically only in the region close to the process zone (i.e. region 1), yielding a smooth plastic curvature profile in region 2, consistent with assumption 3. The curvature graph also shows that the size and the shape of the fully developed process zone (region 1) stays constant with respect to the crack tip location and simply traverses with further growth of delamination from the point of unloading of cycle 1 to that of unloading of cycle 2, i.e. supporting the necessary condition of constant process zone geometry. Additionally, the crack opening displacement (COD) profiles of MB4 at different loading displacements have been horizontally shifted to a single crack tip location to show that the process zone geometry remains unchanged during crack propagation, see Fig. 11.

Since the assumptions made in the previous section have been numerically verified for the considered material/geometry parameter set, the proposed approach is next applied to a numerical problem for which both structural and interface plasticity are present.

### 3.3 Numerical verification of the full approach

Using the area  $ACDB$  from the load–displacement curve of MB4 (Fig. 12) for which both structural and

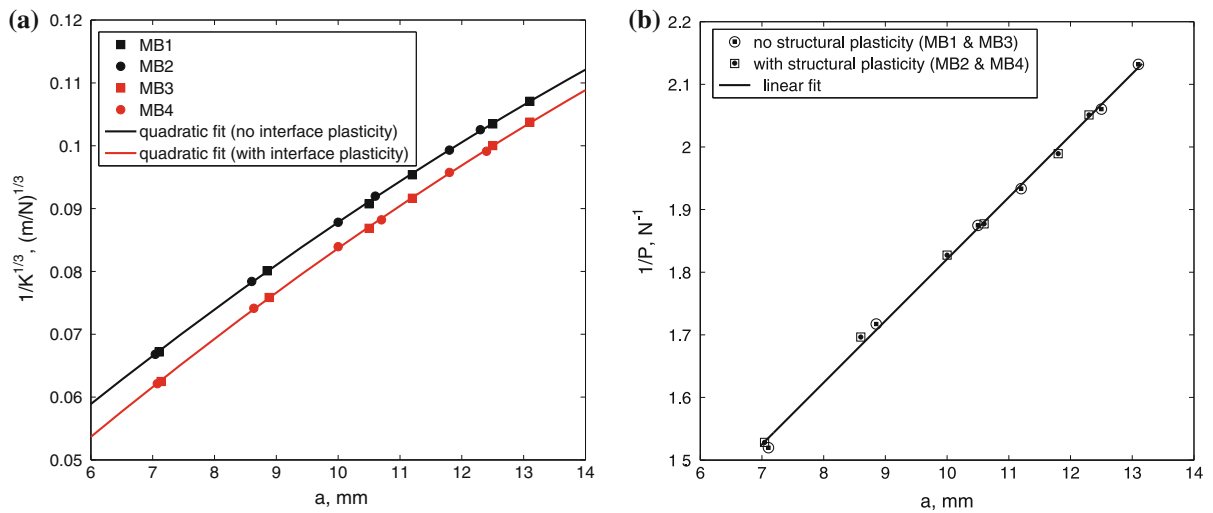


**Fig. 9** **a** The global unloading stiffness,  $K$ , and the corresponding crack lengths  $a$  at each opening displacement are plotted as  $\frac{1}{K^{1/3}}$  versus  $a$  for all four classes of interface and bulk structural material behavior given in Table 1. The same (quadratic) dependency identified for cases without (MB1 and MB3) and with

(MB2 and MB4) structural plasticity supports the assumption 1. **b** The inverse of the critical load points  $1/P$  of the delamination curve plotted as a function of the corresponding crack lengths  $a$  for cases without (MB1 and MB3) and with structural (MB2 and MB4) plasticity in order to verify assumption 2

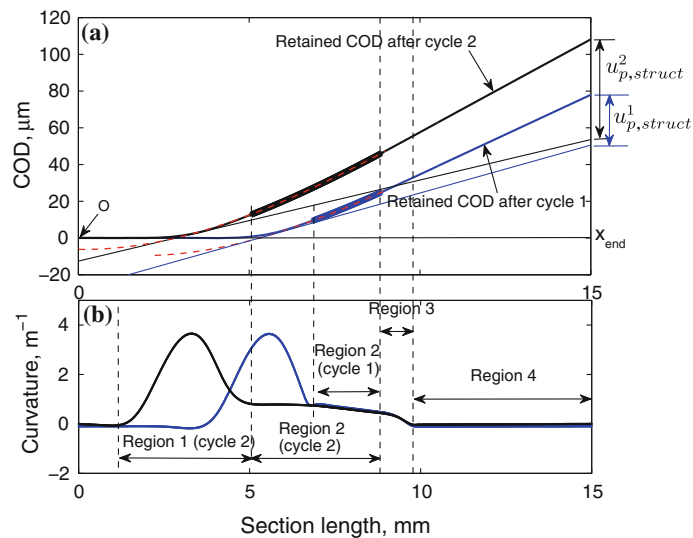


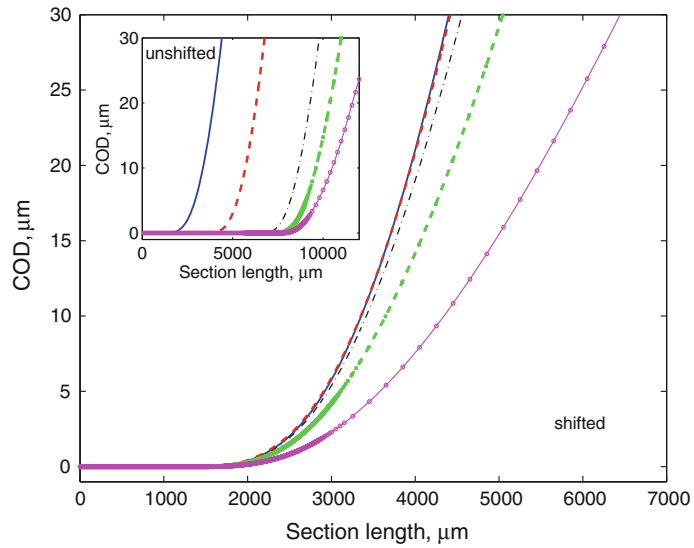
**Fig. 10** **a** Retained crack opening displacement (COD) profiles after complete unloading of cycle 1 and cycle 2 for the case of MB4 (both interface and structural plasticity), and **b** corresponding curvature plots illustrating the four different regions. **b** Shows that the size and shape of the (fully developed) process zone remain constant with respect to the crack tip position during

crack growth from cycle 1 to cycle 2, while the plastic curvature in region 2 stays nearly constant in time and place. **a** Also shows the procedure to obtain the contribution of structural plasticity to the retained opening for cycle 1 and cycle 2 (i.e.  $u_{p,struct}^1$  and  $u_{p,struct}^2$ , respectively) using the proposed approach

interface plasticity are present, an interface fracture toughness value of  $6.05 \text{ J/m}^2$  would be obtained without separation of structural plastic contributions. This value is 29% larger than the actual input value of

$4.7 \text{ J/m}^2$ . Therefore, as a verification of the proposed approach, the structural plastic contribution, including the elastic stored energy, to the total work during delamination is separated to assess the obtained value for

**Fig. 11** Numerical crack opening displacement (COD) profiles of MB4 at different loading displacements horizontally shifted to the same crack tip location. The original unshifted profiles are shown in the *inset*. These results show that the crack initiation is followed by a stable crack growth regime in which the process zone remains exactly constant, and thus can be used to determine the fracture toughness from



the interface fracture toughness. The regions 2 of the retained COD profiles corresponding to the unloading of cycle 1 and cycle 2 are fitted with cubic polynomials (as shown in Fig. 10a). Cubic polynomials were selected because the curvature profiles vary nearly linear with section length for both cycles in region 2. The fitted curves are extrapolated into the corresponding region 1 of each cycle to find the intersection points on the axis  $Ox_{end}$ . The tangents drawn at these intersection points are extended to  $x_{end}$  to obtain the retained openings due to structural plasticity,  $u_{p,struct}^1$  and  $u_{p,struct}^2$  of cycle 1 and cycle 2, respectively (Fig. 10a).

As explained in Sect. 2.2, the global unloading stiffness lines corresponding to cycle 1 and cycle 2 are then translated over a distance  $u_{p,struct}^1$  and  $u_{p,struct}^2$  towards the origin to identify the two points,  $A'$  and  $C'$ , (corresponding to  $A$  and  $C$  respectively) on the reconstructed curve. The points  $X'$  between  $A'$  and  $C'$  are obtained by applying a scaled linear interpolation of  $u_{p,struct,X'}$  between  $u_{p,struct}^1$  and  $u_{p,struct}^2$  as explained in Sect. 2.2. Using the area  $A'C'D'B'$  from the reconstructed curve (Fig. 12), an interface fracture toughness of  $4.82 \text{ J/m}^2$  is obtained which is in good agreement with the input value of  $4.70 \text{ J/m}^2$ . The small deviation is caused by a slight mixed mode loading as explained next.

In order to further validate the approach, a comparison is made between on one hand the structural plastic dissipation (including the stored elastic energy) that is determined by the numerical integration of energies in sample structure and on the other hand the energy

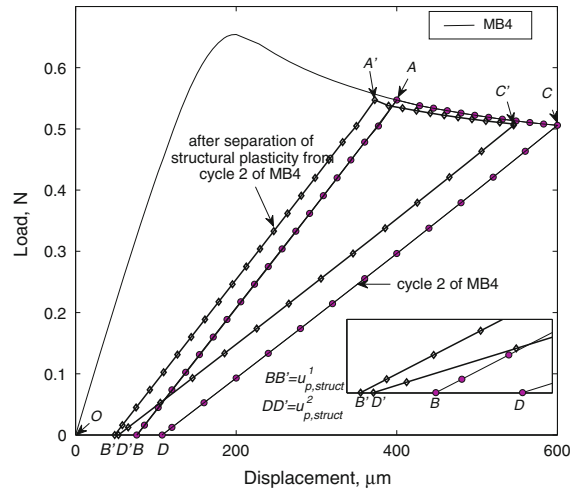


**Fig. 12** Load–displacement response for MB4 (structural and interface plasticity). The structural plastic contribution is separated from the total dissipated energy ( $ACDB$ ) for MB4 by employing the procedure described in Sect. 2.2 (i.e. by reconstructing  $A'C'D'B'$ )

that is dissipated or stored in the sample structure during one loading–crack growth–unloading cycle, as determined by the presented practical approach, and therefore excluded from the fracture toughness. Table 3 shows this analysis and the corresponding fracture toughness values determined for all the four classes of interface and bulk structural material behavior considered in this research. For both cases involving structural plasticity (MB2 and MB4), this analysis shows that the dissipated or stored energy in the sample structure

**Table 3** Numerical validation of the energy balance for all the four classes of interface and bulk structural material behavior

Class	MB1	MB2	MB3	MB4
Mode I fracture toughness, $J/m^2$ (simulation input)	4.7	4.7	4.7	4.7
Structural plastic dissipation during a loading–crack growth–unloading cycle, $J \times 10^{-6}(A)$	0	11.7	0	11.7
Change in stored elastic energy between two consecutive unloadings, $J \times 10^{-6}(B)$	0	2.1	0.4	2.5
$A + B, J \times 10^{-6}$	0	13.8	0.4	14.2
Energy dissipated or stored in the sample structure, as determined with the practical approach, $J \times 10^{-6}$	0	13.2	0	14.1
Total work done/unit area of crack extension in a loading–crack growth–unloading cycle, $J/m^2$	4.82	5.98	4.83	6.05
Fracture toughness, as determined with the practical approach, $J/m^2$	4.82	4.83	4.83	4.82

that is identified by the presented approach (row 6), is matching well with the sum of the plastic dissipation and change in stored elastic energy, determined by the numerical integration (row 5). This is because the present approach relies on using retained curvature of the sample structure, which is the result of the combined effect of structural plasticity and associated stored elastic energy, for the compensation of the structural plasticity. For the cases where there is no structural plastic dissipation (MB1 and MB3), the fracture toughness is determined directly using the total work done in a loading–crack growth–unloading cycle as it is normally done in a delamination growth experiment. For these cases, the change in elastically stored energy associated with interface plasticity is negligible because of the constant process zone geometry during crack propagation. Finally, in all the numerical simulations, the extracted interface fracture toughness (row 8) matches well with the known (input) mode-I fracture toughness of the CZ model (row 2). In fact, detailed numerical analysis showed that the small systematic difference (4.7 vs. 4.8), that exists even for the case with no plasticity at all (MB1), is caused by a small mode II component (mode angle of  $\sim 1^\circ$ ) to the extracted interface fracture toughness. In all, this analysis of the evolution of the different sources of energies shows that the practical approach is indeed able to separate the effects of the interface fracture and the structural plasticity once the conditions for applicability of this practical approach are met. Finally, it should be noted that this numerical analysis has only been performed for one material/geometry parameter set, therefore, further research is needed to assess the limits of applicability of the approach for a wider range of parameter sets.

#### 4 Experimental assessment on CuLF–MCE interfaces

In this section, the proposed approach for the separation of structural plastic contributions from the measured load–displacement response is experimentally assessed by separating the induced structural plasticity and comparing the resulting interface fracture toughness with the value obtained from another sample of the same interface in which no structural plasticity occurred. Since it is not experimentally possible to switch on and off the plasticity in the process zone and/or sample structure, samples with a different thickness are used to experimentally evaluate the influence of structural plasticity. For this purpose, two identical industrially relevant CuLF–MCE bilayer samples, but with different thickness of the CuLF layer (0.2 mm and 0.15 mm) are chosen. The rest of the dimensions (5 mm width, 35 mm length and 0.5 mm MCE layer thickness) are the same for both samples.<sup>3</sup> The thick CuLF layer shows no structural plasticity, whereas considerable structural plasticity occurs in the thin CuLF sample during delamination. The MCE layer is always elastic in both cases. Unfortunately, for the present case, a comparison between experiments and simulations is not directly possible, because this requires (precise) determination of the bulk constitutive properties of both layers of the interface structure, and the samples are produced by molding the epoxy on the copper sheets, which does

<sup>3</sup> Numerical simulations of both sample structures in the MMB loading setup (not shown here) showed that the difference in mode angle between these two interfaces is less than  $2^\circ$  and that the influence due to this change in mode mixity can be neglected with respect to the measurement uncertainties.

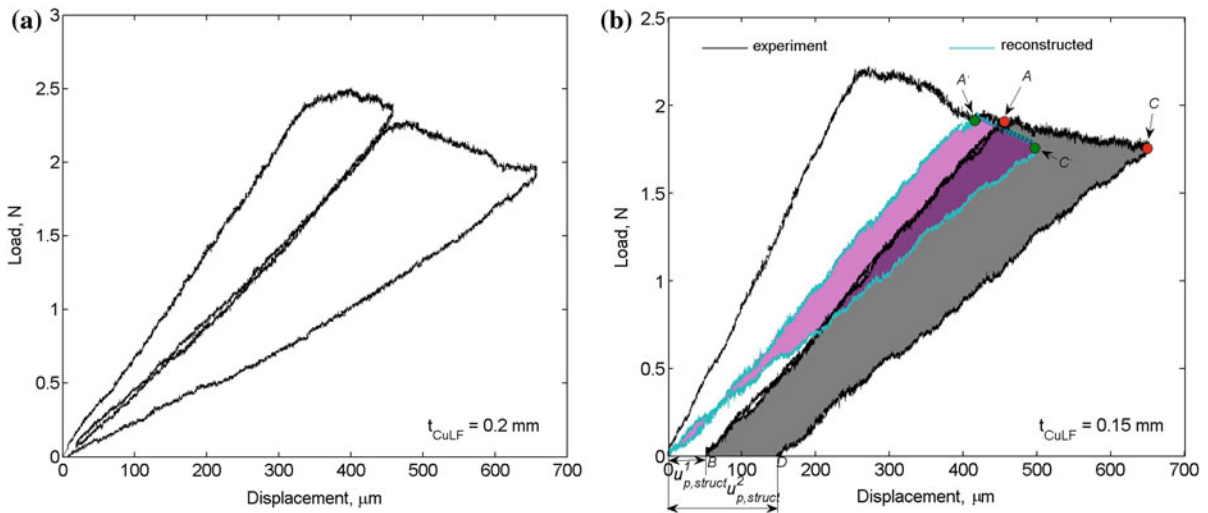


**Fig. 13** Load–displacement response of a mode I delamination experiment conducted on **a** a thick CuLF(0.2 mm)–MCE(0.5 mm) bilayer sample showing negligible retained opening after complete unloading; **b** a thin CuLF(0.15 mm)–MCE(0.5mm) bilayer sample exhibiting a retained structural

not allow to manufacture free-standing MCE samples with exactly the same material behavior.

The load–displacement response of a mode I delamination experiment performed on the thick CuLF–MCE sample is shown in Fig. 13a. From the graph it is clear that there is indeed no observable interface or structural plasticity present in this first experiment. An interface fracture toughness value of  $36 \text{ J/m}^2$  is obtained by simply dividing the energy dissipated in a loading–delamination–unloading cycle with the corresponding increase in crack length and sample width. Note that the first loading–unloading cycle is generally ignored because it includes the crack initiation regime and the development of the process zone. On the other hand, the load–displacement response of a mode I delamination experiment performed on a thin CuLF–MCE sample (black line in Fig. 13b) reveals considerable retained opening after unloading to zero load. The interface fracture toughness value calculated using the total energy spent in the second loading–unloading cycle (area  $BACD$  in Fig. 13b) and the corresponding increase in crack length during this cycle gives a value of  $73 \text{ J/m}^2$  which is more than twice the value measured for the thick copper layer.

For the present situation, it is known that the complete retained opening in Fig. 13b and the additional dissipation originates from plasticity in the layers of

opening. The shaded grey area ( $ACDB$ ) shows the total energy spent during loading–unloading cycle 2. The reconstructed curve with the enclosed magenta filled area ( $O A' C'$ ) shows the delamination energy in cycle 2 after separation of the structural plastic contribution

the sample structure, because there was no interface plasticity observed for the thick CuLF–MCE sample. Nevertheless, the general procedure described for the case of both interface and structural plasticity (see Sect. 2.2) is applied for the separation of the structural plastic contribution.

That means, first the retained COD profiles of the sample after unloading of cycle 1 and cycle 2 to zero load (i.e. at points  $B$  and  $D$  in Fig. 13b) are obtained by digital image correlation (DIC) analysis of images of the sample taken before the start and after each cycle of the delamination test. To obtain a random pattern that allows for accurate image correlation, the surface of each sample is carefully polished after which silver nano-particles (with a size of 50–100 nm) are applied before the beginning of the actual delamination test. The micrograph of the retained opening profile with the DIC measured displacement field overlay and the corresponding COD profile after unloading of cycle 2 are shown in Fig. 14. Region 2 (identified as outlined in Sect. 3.3) of the measured COD profiles are fitted accurately ( $R^2 > 0.9995$ ) with cubic polynomials and extrapolated into region 1 onto the axis  $Ox$ . The polynomial fit extrapolated to  $Ox$  for the unloaded COD profile (cycle 2) are shown in the middle figure of Fig. 14. It should be noted that the error between the measured COD profile and the fitted curve in region

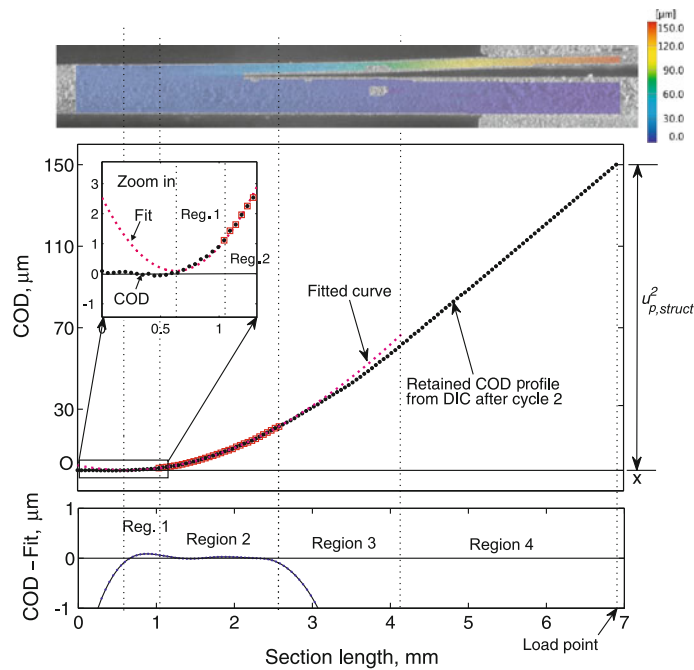


**Fig. 14** A micrograph of the sample taken after complete unloading of cycle 2 with a digital image correlation (DIC) displacement field overlay is shown in the *top figure*. The retained crack opening displacement (COD) profile measured (by DIC analysis) for the sample after complete unloading of cycle 2, and

the different regions are shown in the *middle figure*. The error in the cubic polynomial fit of region 2 as a function of the section length is shown in the *bottom figure*. It can be observed that the polynomial fit matches the COD data with an error of less than  $0.1 \mu\text{m}$  over the full length of region 2

2 is noticeably small as shown in the bottom graph of Fig. 14, which shows that the plastic curvature profile is smooth, in agreement with assumption (3) in Sect. 3.2. The extrapolated cubic polynomial curve (nearly) touches the axis  $Ox$  with an almost zero slope (lowest point in the zoom box of Fig. 14) confirming that, indeed, there is only structural plasticity present during this delamination experiment. Accordingly, the identified values of  $u_{p,struct}^1 = 50 \mu\text{m}$  and  $u_{p,struct}^2 = 150 \mu\text{m}$  are exactly the same as the global retained openings  $u_p^1$  and  $u_p^2$  found from the load–displacement graph after unloading of each cycle. Subsequently, the global unloading stiffness lines  $AB$  and  $CD$  are translated towards the origin over a distance  $u_{p,struct}^1$  and  $u_{p,struct}^2$  (or  $OB$  and  $OD$ ) to identify the two points  $A'$  and  $C'$  on the reconstructed curve, respectively. The points in between  $A'$  and  $C'$  on the reconstructed curve are obtained by using the scaled linear interpolation function described in Sect. 2. The area surrounded by the curves  $OA'C'$  corresponds to the energy spent for interface delamination excluding structural plasticity contributions. The fracture toughness value obtained is

$31 \text{ J/m}^2$  which is in adequate agreement with the value of  $36 \text{ J/m}^2$  for the thick CuLF–MCE sample without observable structural plasticity and which is less than 50% of the value ( $73 \text{ J/m}^2$ ) obtained before application of the structural plasticity separation method. The remaining deviation ( $36$  vs.  $31 \text{ J/m}^2$ ) is attributed to measurement uncertainties in the delamination experiment (load, displacement and crack length measurements), possible anticlastic deformation of the structural layers causing errors in DIC COD profiles, statistical differences in the interface behavior of the two different sample (although they are from the same batch), and the model approximations made. The small error involved in fitting the plastically deformed region (region 2) contributes negligibly to the observed deviation. Finally, the change in the process zone geometry is assessed to certify the validity of the approach. In Fig. 15 the COD profiles of the thin CuLF–MCE sample at different opening displacements are presented to show that the process zone remains constant for the structures. Although the change in the process zone size was found to be negligible for the test example, this may



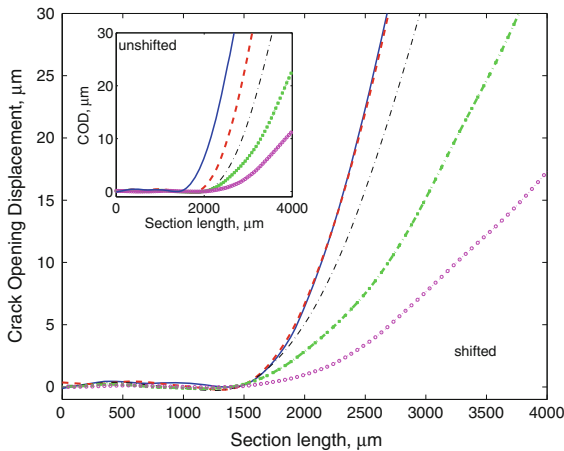


**Fig. 15** Experimental crack opening displacement (COD) profiles of a CuLF–MCE sample at different loading displacements horizontally shifted to the same crack tip (the original unshifted profiles are shown in *inset*), which again show that the process zone remains exactly constant in the stable crack growth regime from which the fracture toughness can thus be determined

not be the case in general (see, e.g. [Suo and Fan 1992](#)). Therefore, the experimentalist should always check this requirement before the application of the proposed procedure. As a conclusion, it can be stated that, if ignored, the structural plastic deformation of the sample layers during delamination can introduce large errors in the measurement of the interface fracture toughness.

## 5 Conclusions

Delamination characterization of multi-layer structures containing ductile layers is challenging because of the occurrence of permanent deformation of the adherent layers of the sample structure during delamination. Large errors in the measurement of the interface fracture toughness can result if these structural plastic dissipations are neglected in the calculation of the interface fracture toughness. Therefore, a practical approach accounting for the structural plasticity in the adherent layers of the sample is proposed, aiming for accurate values of the mode I interface fracture toughness in a delamination growth experiments involving small-scale plasticity in connection with ductile interface fracture and structural plasticity in the adherents induced by beam bending. The approach relies on the reconstruction of the equivalent force–displacement curve for the no structural plasticity case, departing

from the measured force–displacement response. Individual contributions of structural plasticity and interface plasticity to the total retained opening are identified after complete unloading of the sample. This is achieved by assuming that both the global unloading stiffness and the critical load for delamination (for a given crack length) are not affected by permanent deformation of the sample structure. The partitioning of the individual contributions of structural plasticity and interface plasticity to the total retained opening is achieved by utilizing measured retained crack opening profiles of the sample. This procedure assumes a smooth plastic curvature profile in the delaminated beams. For the validity of this approach the geometry of the process zone should remain unchanged during crack propagation, which is in any case a necessary condition for delamination growth type of experiments.

The proposed approach and its underlying assumptions have been numerically verified for one set of parameters by employing a finite element model with a known cohesive zone response at the interface. In this verification, the structural plastic contribution to the dissipated energy was successfully separated from a numerical simulation of a delamination experiment where both structural and interface plasticity are present, thereby recovering the correct value for the interface fracture toughness. Energy validation by numerical analysis showed that the dissipated and stored energy in the sample structure, determined by the presented approach, is matching well with the sum of the plastic dissipation and change in stored elastic energy, as determined by numerical integration. The proposed approach was also assessed experimentally by characterizing the interface fracture toughness of industrially relevant CuLF–MCE samples. In this example, it was found that a correction of the interface fracture toughness of more than a factor of two results by applying the proposed approach.

Although, future work is needed for the numerical validation of the approach over wide range of parameter sets, the presented approach is still relevant for the micro-electronics community and a valuable step forward to deal with the structural plasticity problem in a delamination characterization experiment. Moreover, the approach does neither require an analytical solution or numerical simulation nor the explicit details of the constitutive behavior of the adherents. Finally, it is noted that the proposed approach can only be used to compensate for energy dissipation due to structural

plasticity leading to a permanent curvature and it is not applicable when the structural arms of the sample undergo plastic deformation during unloading (i.e. reverse plasticity) and when there are any dissipative mechanisms causing non-negligible hysteresis in the global un- and reloading response.

**Acknowledgments** This research was carried out under the project number MC2.05235 in the framework of the research program of the Materials innovation institute M2i ([www.m2i.nl](http://www.m2i.nl)). The authors are grateful to Marc van Maris for his assistance in conducting experiments. Peter Timmermans and Olaf van der Sluis from Philips are acknowledged for their help in manufacturing and supply of the samples.

## References

- Andersson T, Stigh U (2004) The stress–elongation relation for an adhesive layer loaded in peel using equilibrium of energetic forces. *Int J Solids Struct* 41:413–434
- Biel A, Stigh U (2010) Damage and plasticity in adhesive layer: an experimental study. *Int J Fract* 165:93–103
- Blanco N, Turon A, Costa J (2006) An exact solution for the determination of the mode mixture in the mixed-mode bending delamination test. *Compos Sci Technol* 66:1256–1258
- Davidson BD, Sundararaman V (1996) A single leg bending test for interfacial fracture toughness determination. *Int J Fract* 78:193–210
- Davies GAO, Hitchings D, Ankersen J (2006) Predicting delamination and de-bonding in modern aerospace composite structures. *Compos Sci Technol* 66:846–854
- Kim JK, Mai YW (1991) High strength, high fracture toughness fibre composites with interface control—a review. *Compos Sci Technol* 41(4):333–378
- Kolluri M (2011) An in-situ experimental-numerical approach for interface delamination characterization. PhD thesis, Eindhoven University of Technology, Netherlands. ISBN: 978-90-77172-75-9
- Kolluri M, Thissen MHL, Hoefnagels JPM, van Dommelen JAW, Geers MGD (2009) In-situ characterization of interface delamination by a new miniature mixed mode bending setup. *Int J Fract* 158:183–195
- Kolluri M, Hoefnagels JPM, van Dommelen JAW, Geers MGD (2011) An improved miniature mixed mode delamination setup for in-situ microscopic interface failure analyses. *J Phys D Appl Phys* 44:1–13
- Rikards R, Buchholz FG, Wang H, Bledzki AK, Korjakin A, Richard HA (1998) Investigation of mixed mode I/II interlaminar fracture toughness of the laminated composites by using a CTS type specimen. *Eng Fract Mech* 61:325–342
- Salomonsson K, Stigh U (2008) An adhesive interphase element for structural analyses. *Int J Numer Methods Eng* 76:482–500
- Soboyejo WO, Lu GY, Chengalva S, Zhang J, Kenner V (1999) A modified mixed-mode bending specimen for the interfacial fracture testing of dissimilar materials. *Fatigue Fract Eng Mater Struct* 22:799–810
- Suo Z, Bao G, Fan B (1992) Delamination r-curve phenomena due to damage. *J Mech Phys Solids* 40:1–16
- Thijssse J, van der Sluis O, van Dommelen JAW, van Driel WD, Geers MGD (2008) Characterization of semiconductor interfaces using a modified mixed mode bending apparatus. *Microelectron Reliab* 48:401–407
- Thouless MD, Kafkalidis MS, Adams JL, Ward SM, Dickie RA, Westerbeek GL (1998) Determining the toughness of adhesives in plastically-deforming joints. *J Mater Sci* 33:189–197
- Todoroki A, Tanaka M, Shimamura Y (2005) Electrical resistance change method for monitoring delamination of CFRP laminates: effect of spacing between electrodes. *Compos Sci Technol* 65:37–46
- Tvergaard V, Hutchinson JW (1992) The relation between crack growth resistance and fracture process parameters in elastic–plastic solids. *J Mech Phys Solids* 40:1377–1397
- Tvergaard V, Hutchinson JW (1993) The influence of plasticity on mixed mode interface toughness. *J Mech Phys Solids* 41:1119–1135
- Tvergaard V, Hutchinson JW (1996) On the toughness of ductile adhesive joints. *J Mech Phys Solids* 44:789–800
- van der Sluis O, Engelen RAB, van Silfhout RBR, van Driel WD, van Gils MAJ (2007) Efficient damage sensitivity analysis of advanced Cu/low-k bond pad structures by means of the area release energy criterion. *Microelectron Reliab* 47:1975–1982
- van Driel WD, van Gils MAJ, van Silfhout RBR, Zhang GQ (2005) Prediction of delamination related IC and packaging reliability problems. *Microelectron Reliab* 45:1633–1638
- Valoroso N, Fedele R (2010) Characterization of a cohesive-zone model describing damage and de-cohesion at bonded interfaces. sensitivity analysis and mode-I parameter identification. *Int J Solids Struct* 47:1666–1677
- Wei Y, Hutchinson JW (1997) Nonlinear delamination mechanics for thin films. *J Mech Phys Solids* 45:1137–1159
- Wei Y, Hutchinson JW (1998) Interface strength, work of adhesion and plasticity in the peel test. *Int J Fract* 93:315–333
- Yang QD, Thouless MD, Ward SM (1999) Numerical simulations of adhesively-bonded beams failing with extensive plastic deformation. *J Mech Phys Solids* 47:1337–1353
- Yang QD, Thouless MD (2001) Mixed-mode fracture analyses of plastically-deforming adhesive joints. *Int J Fract* 110:175–187